Fast realization of high-fidelity nonadiabatic holonomic quantum gates with a time-optimal-control technique in Rydberg atoms

P.-Y. Song,[1] J.-F. Wei,[1] Peng Xu,[1,5,*] L.-L. Yan,[1,5] M. Feng,[2,3,4] Shi-Lei Su,[1,5,†] and Gang Chen[1,‡]

[1]*School of Physics, Key Laboratory of Materials Physics of Ministry of Education, and International Laboratory for Quantum Functional Materials of Henan, Zhengzhou University, Zhengzhou 450001, China*

[2]*State Key Laboratory of Magnetic Resonance and Atomic and Molecular Physics, Wuhan Institute of Physics and Mathematics, Innovation Academy of Precision Measurement Science and Technology, Chinese Academy of Sciences, Wuhan 430071, China*

[3]*School of Physics, University of the Chinese Academy of Sciences, Beijing 100049, China*

[4]*Research Center for Quantum Precision Measurement, Institute of Industry Technology, Guangzhou and Chinese Academy of Sciences, Guangzhou 511458, China*

[5]*Institute of Quantum Materials and Physics, Henan Academy of Science, Henan 450046, China*

(Received 13 July 2023; accepted 30 January 2024; published 20 February 2024)

The nonadiabatic holonomic quantum computation (NHQC) has received great attention for decades, however, there are many challenges to its implementation in experiments. To further shorten the evolution time is the first challenge to be conquered to realize high-fidelity quantum gates in NHQC. In this paper, we propose a controlled two-qubit model in Rydberg atoms to realize nonadiabatic holonomic quantum gates, where the evolution time is extremely decreased and the influences of several kinds of noises are minimized by utilizing the time-optimal-control technique on the target atom. In addition, we can construct arbitrary geometric gates by selecting the appropriate parameters in our model. Furthermore, numerical simulations for the C-T gate and C-$\sqrt{H}$ gate based on the master equation show that the fidelities of geometric gates obtained in our model are still very high even though noises are considered, which demonstrates the robustness of our protocol. It is worth noting that the controlled two-qubit model may pave the way to realize fault-tolerant quantum computation in the future.

DOI: 10.1103/PhysRevA.109.022613

I. INTRODUCTION

Since Shor has proved that quantum computation can be used to efficiently solve large-number factorization in 1994 [1], this area has received great attention and has been developed rapidly. A key challenge in this area is to realize fast implementations of quantum gates that are resilient to various kinds of noises. Holonomic quantum computation (HQC) is a general protocol to construct robust quantum gates because the holonomic phase only depends on global properties of the evolution path and is insensitive to the evolution details [2–4]. However, HQC is based on adiabatic evolution, which means that, in general, it requires a very long time for operating systems to achieve goals. Inevitably, the fidelity of quantum gates must be decreased because of accumulation of relaxation, dephasing, imperfect quantum manipulation, and other decohered channels [5–7]. Therefore, fighting against various noises and operation errors is essential to achieve high-fidelity quantum manipulation. To shorten the evolution time and suppress these decohered channels, nonadiabatic holonomic quantum computation (NHQC) based on nonadiabatic non-Abelian geometric phase [8] has been proposed [9,10], not only avoids the disadvantage of long-time evolution but also maintains the advantage of geometric phase [11] which are robust against control errors. So far, this protocol has been implemented experimentally in many systems, such as nitrogen-vacancy centers in diamond [12–17], ion trap systems [18], nuclear magnetic resonance system [19–21], superconductivity systems [22–24], and so on.

In contrast to the platforms mentioned above, the Rydberg atom, where the external electron is excited to high-lying states, also can be used to encode quantum information or realize single-qubit quantum gates due to their long lifetime [25–31]. Furthermore, Rydberg atoms exhibit large dipole moments such that there are strong van der Waals or dipole-dipole interactions [25,32–43], which provides us with a direct way to realize two-qubit controlled quantum gates based on NHQC [44–47]. However, the implementation of the conventional NHQC must satisfy strict conditions, and the same long evolution time is required to realize the arbitrary geometric gate at any angle, which will lead to its sensitivity to decoherence effects [48–50].

In this article, we propose an efficient two-qubit controlled model by utilizing the dipole-dipole interaction between Rydberg atoms, combined with the time-optimal-control (TOC) technique, which can further shorten the evolution time by solving the quantum brachistochrone equation (QBE) [51–56]. Thus, an arbitrary universal quantum gate with high fidelity can be realized by changing the laser amplitude and phase parameters (we also realize the single-qubit gate based on TOC in Appendix A). Here we stress that our work is

*physicalxupeng@whu.edu.cn
†slsu@zzu.edu.cn
‡chengang971@163.com

different from the previous papers [20,57–64]. In Ref. [57], the authors took advantage of adiabatic, shortcut-to-adiabaticity (STA), and nonadiabatic methods to construct the Rydberg gates. For the STA case, they set the amplitude and detuning of the original coupling laser as being time-dependent. While for our scheme the QBE-based TOC is employed to achieve Rydberg quantum computation in the shortest evolution time compared with the STA scheme, and we provide the analytic solutions for the phase and the shortest evolution time in the effective three-level system by solving QBE. In addition, for the parameters only the phase of the effective Rabi frequency is set as time dependent. We set the laser detuning equal to the fixed Förster defect, which is crucial for achieving the holonomic quantum gate without the need for additional resources or operations to realize the time-dependent detuning [65]. Also, the authors of Refs. [58,59] focused on a different topic, i.e., the Rydberg blockade [66]. Furthermore, our model combines a TOC technique, finding a shorter evolution path on the Bloch sphere than those found in Refs. [20,60–64], where there are single-loop protocols and they are sensitive to decoherence errors. In this work, we also numerically simulate the effects of external field noises, including the Rabi frequency error, detuning error, and laser phase noise, as well as the effect of intrinsic Rydberg atom noises, including Doppler dephasing and spontaneous emission. To demonstrate the robustness of our scheme, we compare the numerical simulation results of our scheme with that of the conventional NHQC and shortcuts to adiabaticity (STA) [67] schemes. Finally, the theoretical analysis and the numerical simulations show that our proposal is efficient and robust to generate two-qubit quantum gates based on the time-optimal-control NHQC (TONHQC).

The rest of this article is organized as follows. In Sec. II, we depict the model and the two-qubit effective Hamiltonians. In Sec. III, the theoretical framework for the TOC technique to realize arbitrary holonomic gates has been illustrated. In Sec. IV, we numerically simulate the average fidelity of quantum gates considering the several decoherence channels and compare the robustness of our scheme with the conventional NHQC and STA. Finally, we summarize our results in Sec. V.

II. MODEL AND EFFECTIVE HAMILTONIANS

We consider two cesium atoms trapped in optical tweezers as shown in Fig. 1(a), and the distance between two atoms can be easily adjusted in current experiments. Conveniently, the left atom is called the control atom, while the right one is called the target atom. The energy levels for both atoms are depicted in Fig. 1(b). The hyperfine ground states $|0\rangle_{c,t} = |6S_{1/2}, F = 3, m_F = 0\rangle$ and $|1\rangle_{c,t} = |6S_{1/2}, F = 4, m_F = 0\rangle$ are chosen as the qubit-state because they are resilient to external magnetic fields. The state $|1\rangle_{c,t}$ can be coupled with a Rydberg state $|r\rangle_{c,t}$ by a two-photon resonant laser with Rabi frequency $\Omega_c(t)$ for the control atom and a two-photon off-resonant laser with Rabi frequency $\Omega_1 e^{i\phi_1(t)}$ and detuning Δ for the target atom. The state $|0\rangle_t$ is also coupled with $|r\rangle_t$ for the target atom by a two-photon off-resonant laser with Rabi frequency $\Omega_0 e^{i\phi_0(t)}$ and detuning Δ. In addition, there exists another pair of Rydberg states $|u\rangle_c$ and $|v\rangle_t$ such that the dipole interaction between these two atoms is not negligible

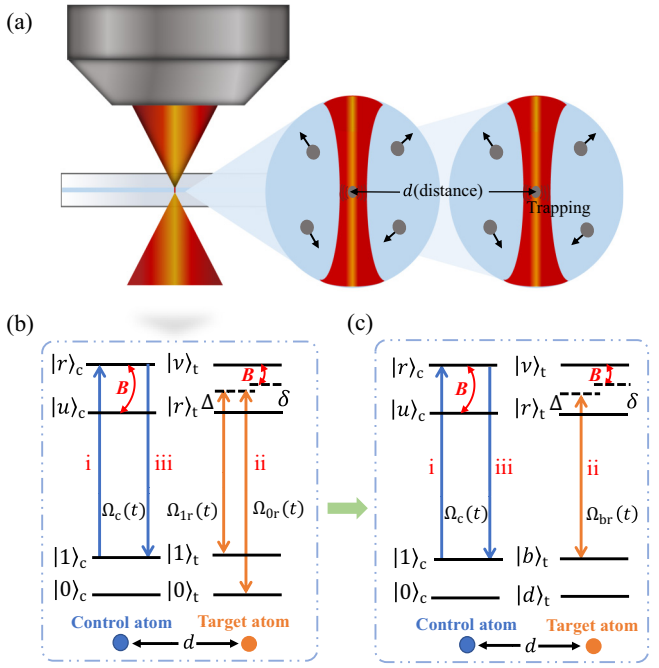

FIG. 1. (a) Schematics of atoms trapped in optical tweezers. (b) Three steps for realization of NHQC: The ground state $|1\rangle_c$ is resonantly excited to the Rydberg state $|r\rangle_c$ with real Rabi frequency $\Omega_c(t)$ in (i) and deexcitation in (iii), while the ground state $|0\rangle_c$ is decoupled from the dynamics; (ii) both $|0\rangle_t$ and $|1\rangle_t$ are coupled to the Rydberg state $|r\rangle_t$ with time-dependent Rabi frequencies $\Omega_{0r}(t)$ and $\Omega_{1r}(t)$, respectively, and with blue detuning Δ. The strength of dipole interaction between two atoms is B. Förster defect in Rydberg states is denoted by δ. Ground states $|0\rangle_t$ and $|1\rangle_t$ can be transformed into a bright state $|b\rangle_t$ and a dark state $|d\rangle_t$ by a unitary transformation such that $|b\rangle_t$ is coupled to $|r\rangle_t$ with Rabi frequency $\Omega_{br}(t)$ and blue detuning Δ while $|d\rangle_t$ is not coupled to other energies. $\Omega_{0r}(t) = \Omega_0 e^{i\phi_0(t)}$, $\Omega_{1r}(t) = \Omega_1 e^{i\phi_1(t)}$, $\Omega_{br}(t) = \Omega_b e^{-i\phi_1(t)}$.

and the strength of the dipole interaction is labeled as B. Here we choose $|r\rangle_c = |85P_{1/2}, m_J = 1/2\rangle$, $|u\rangle_c = |85S_{1/2}, m_J = 1/2\rangle$, $|r\rangle_t = |80P_{3/2}, m_J = 1/2\rangle$, and $|v\rangle_t = |81S_{1/2}, m_J = 1/2\rangle$ [68]. The Förster defect δ can be calculated by the ARC open-source library approximately as $2\pi \times 290$ MHz [69]. To realize universally robust quantum gates, in the following, we discuss two kinds of effective Hamiltonian based on the initial state of the control atom.

First, when the control atom initially stays at $|1\rangle_c$, it can be excited to $|r\rangle_c$ by applying a π pulse, i.e., $\int \Omega_c(t)dt = \pi$, then the Hamiltonian of the system in the interaction picture is described by

$$\hat{H}_1 = \tfrac{1}{2}(\Omega_{1r}(t)|r1\rangle\langle rr|e^{i\Delta t} + \Omega_{0r}(t)|r0\rangle\langle rr|e^{i\Delta t}) + B|rr\rangle\langle uv|e^{-i\delta t} + \text{H.c.}, \quad (1)$$

with Rabi frequencies $\Omega_{0r}(t) = \Omega_0 e^{i\phi_0(t)}$, $\Omega_{1r}(t) = \Omega_1 e^{i\phi_1(t)}$, in which the amplitude of driving field $\Omega_{0(1)}$ is time independent and the phase $\phi_{0(1)}(t)$ is time dependent, blue detuning Δ, dipole-dipole interaction strength B, and the energy defect δ, as shown in Fig. 1(b). It should be noted that the left (right) qubit represents the control (target) atom in the two-qubit basis. Furthermore, the above Hamiltonian can be transformed

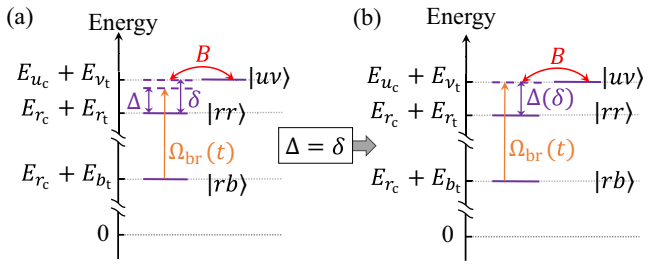

FIG. 2. Level structure of the scheme. The detuning of laser Δ is set equal to the defect of Förster resonance δ of the selected Rydberg states.

into a new basis

$$\hat{H}_1 = \tfrac{1}{2}\Omega_b e^{-i\phi_1(t)}|rr\rangle\langle rb|e^{-i\Delta t} + B|rr\rangle\langle uv|e^{-i\delta t} + \text{H.c.}, \quad (2)$$

where $|b\rangle_t = \sin(\theta/2)e^{i\phi}|0\rangle_t + \cos(\theta/2)|1\rangle_t$ is the bright state that is coupled to the Rydberg state $|r\rangle_t$, while there is a dark state $|d\rangle_t = \cos(\theta/2)|0\rangle_t - \sin(\theta/2)e^{-i\phi}|1\rangle_t$ that is orthogonal to $|b\rangle_t$ but is decoupled from the dynamics. Here, we set the angle θ and phase ϕ to be time independent. We assume $\Omega_b = \sqrt{\Omega_0^2 + \Omega_1^2}$, which is time independent, $\Omega_0/\Omega_1 = \tan(\theta/2)$, $\phi = \phi_0(t) - \phi_1(t)$, and we set $\Delta = \delta$. When $\Delta \gg \Omega_b$ holds, we obtain an effective Hamiltonian for the system according to the Floquet expansion [70]

$$\begin{aligned}\hat{H}_{1,\text{eff}} = &\left(\frac{B\Omega_b}{2\Delta}e^{i\phi_1(t)}|rb\rangle\langle uv| + \text{H.c.}\right)\\ &+ \frac{\Omega_b^2}{4\Delta}(|rb\rangle\langle rb| - |rr\rangle\langle rr|)\\ &+ \frac{B^2}{\Delta}(|uv\rangle\langle uv| - |rr\rangle\langle rr|). \end{aligned} \quad (3)$$

The transition between $|rb\rangle$ and $|uv\rangle$ can be seen as a two-photon resonance process and satisfies energy conservation as shown in Fig. 2.

Second, when the control atom initially stays at $|0\rangle_c$, it cannot be excited to the Rydberg state $|r\rangle_c$, then there is no dipole interaction between these two atoms. So the Hamiltonian of the system is

$$\hat{H}_2 = \tfrac{1}{2}(\Omega_{0r}(t)|0r\rangle\langle 00|e^{-i\Delta t} + \Omega_{1r}(t)|0r\rangle\langle 01|e^{-i\Delta t} + \text{H.c.}). \quad (4)$$

The effective Hamiltonian for this situation yields

$$\hat{H}_{2,\text{eff}} = \frac{\Omega_b^2}{4\Delta}(|0b\rangle\langle 0b| - |0r\rangle\langle 0r|). \quad (5)$$

Note that the Stark shift terms in Eqs. (3) and (5) can be canceled by inducing an opposite Stark shift with an additional laser experimentally [71–75]. Consequently, the system's dynamics for step (ii) after the control atom is excited in step (i) can be described by the Hamiltonian

$$\hat{H}_{\text{eff}} = \frac{B\Omega_b}{2\Delta}e^{i\phi_1(t)}|rb\rangle\langle uv| + \text{H.c.}. \quad (6)$$

III. TIME-OPTIMAL-CONTROL NHQC

To construct fast high-fidelity and robust quantum gates, the essential step is to find an optimal-control trajectory. Experimentally, the arbitrary holonomic gate can be realized by tuning parameters $\phi_1(t)$, while the values of Ω_b, Δ, and B are kept constant. In the following, we will explain this scheme in detail.

Generally, for an arbitrary state $|\psi_m(t)\rangle$ satisfying the Schrödinger equation, i.e., $i|\dot{\psi}_m(t)\rangle = \hat{H}(t)|\psi_m(t)\rangle$, the evolution operator can be formally written as $\hat{U}(\tau) = \sum_k |\psi_k(\tau)\rangle\langle\psi_k(0)|$. Here we induce a set of auxiliary bases $\{|\Psi_m(t)\rangle\}$, which satisfy the periodic boundary condition and do not have to be the solutions of the Schrödinger equation such that $|\Psi_m(\tau)\rangle = |\Psi_m(0)\rangle = |\psi_m(0)\rangle$. After one period, the evolution operator is written as $\hat{U}(\tau) = \sum_{lk}[Te^{i\int_0^\tau (D+G)\,dt}]_{lk}|\psi_l(0)\rangle\langle\psi_k(0)|$, with the dynamical part $D_{lk} = -\langle\Psi_l(t)|\hat{H}(t)|\Psi_k(t)\rangle$ and the geometric part $G_{lk} = \langle\Psi_l(t)|i(d/dt)|\Psi_k(t)\rangle$. By means of the auxiliary bases $\{|\Psi_m[\mu_a(t), \xi_b(t)]\rangle\}(a, b, \ldots, n)$ with two sets of independent parameters $\mu_a(t)$ and $\xi_b(t)$, the geometric part is expressed as $G_{lk} = G^{\mu}_{lk} + G^{\xi}_{lk}$ with $G^{\mu}_{lk} = \sum_a i\langle\Psi_l(t)|\partial/\partial\mu|\Psi_k(t)\rangle(d\mu_a/dt)$ and $G^{\xi}_{lk} = \sum_b i\langle\Psi_l(t)|\partial/\partial\xi|\Psi_k(t)\rangle(d\xi_b/dt)$ [8]. Furthermore, the dynamical part exactly cancels with G^{ξ}_{lk}, i.e., $D_{lk} + G^{\xi}_{lk} = 0$. One possible general option to satisfy this condition is $\{|\Psi_a[\mu_a(t), \xi_b(t)]\rangle\} = e^{i\mu_a(t)}|\psi_a[\xi_b(t)]\rangle$, in which $|\psi_a[\xi_b(t)]\rangle$ evolves according to the Schrödinger equation. Finally, we obtain the robust geometric phase μ_a, which is independent of the Hamiltonian and only depends on the Hilbert space structure. (Detailed calculations are shown in Appendix B.) Meanwhile, combining with the periodic boundary condition, $\hat{U}(\tau) = \sum_a e^{i\mu_a(\tau)}|\Psi(0)\rangle_a\langle\Psi(0)|$ satisfies the gauge invariance [4], which verifies the geometric properties of holonomic quantum gates.

For the Hamiltonian in Eq. (6), we define $\xi_1(t) = \frac{1}{2}\int\sqrt{\Omega_{\text{eff}}^2 + \dot{\phi}_1^2(t)}dt$, where $\Omega_{\text{eff}} = B\Omega_b/\Delta$ is time independent. Then we can define the general form of three orthogonal bases (i.e., the set vectors $|\psi_m(t)\rangle$ is a completely orthogonal system) that obey the Schrödinger equation as

$$\begin{aligned}|\psi_0\rangle &= \left(\cos\frac{\xi_1}{2} - i\sin\frac{\xi_1}{2}\cos\xi_3\right)\\ &\quad\times e^{-i\frac{\xi_2}{2}}|uv\rangle - i\sin\xi_3\sin\frac{\xi_1}{2}e^{i\frac{\xi_2}{2}}|rb\rangle,\\ |\psi_1\rangle &= -i\sin\xi_3\sin\frac{\xi_1}{2}e^{-i\frac{\xi_2}{2}}|uv\rangle\\ &\quad+\left(\cos\frac{\xi_1}{2} + i\sin\frac{\xi_1}{2}\cos\xi_3\right)e^{i\frac{\xi_2}{2}}|rb\rangle,\\ |\psi_2\rangle &= \cos\frac{\theta}{2}|r0\rangle - \sin\frac{\theta}{2}e^{-i\phi}|r1\rangle. \end{aligned} \quad (7)$$

Here, we set $\xi_3 = \arctan[\Omega_{\text{eff}}/(-\dot{\phi}_1(t))]$ and assuming $\dot{\xi}_3 = 0$ for convenience, which implies $\dot{\phi}_1(t)$ is a constant. Combining Eq. (7) with the Schrödinger equation, we can obtain $\Omega_{\text{eff}} = -2\dot{\xi}_1(t)\sin\xi_3$, $\phi_1(t) = \xi_2(t) = 2\xi_1(t)\cos\xi_3$. To satisfy the cyclic evolution condition, i.e., $\xi_1(0) = \xi_2(0) = 0$, $\xi_1(\tau) = 2\pi$, in computational subspace $\{|\Psi_1(0)\rangle, |\Psi_2(0)\rangle\}$, the evolution operator can be rewritten as

$$\hat{U}(\tau) = e^{i\gamma}|\Psi_1(0)\rangle\langle\Psi_1(0)| + |\Psi_2(0)\rangle\langle\Psi_2(0)|, \quad (8)$$

where the geometric phase is $\gamma = -\mu_1(\tau) + \mu_1(0) = \pi + \xi_2(\tau)/2$. On the bases mentioned above, we can get $\xi_1(t) = -\Omega_{\text{eff}} t/(2\sin\xi_3)$, $\xi_2(t) = -\Omega_{\text{eff}} t/\tan\xi_3$. Considering a π pulse can be applied again to deexcite the control atom, the corresponding evolution operator can be further spanned by the logical qubits $\{|00\rangle, |01\rangle, |10\rangle, |11\rangle\}$,

$$\hat{U}(\tau) = |0\rangle\langle 0| \otimes I + |1\rangle\langle 1| \otimes (e^{i\gamma}|b\rangle\langle b| + |d\rangle\langle d|). \quad (9)$$

Thus, $\hat{U}(\tau)$ can be used to construct arbitrarily controlled two-qubit gates.

In general, the quantum system's errors are proportional to the whole evolution time. Therefore, we can obtain the minimum evolution time by solving the QBE

$$i\partial\hat{F}/\partial t = [\hat{H}_{\text{eff}}, \hat{F}], \quad (10)$$

where $\hat{F} = \partial\hat{L}_c/\partial\hat{H}_{\text{eff}}$, $\hat{L}_c = \sum_j \lambda_j f_j(\hat{H}_{\text{eff}})$, $(j = 1, 2, 3, \ldots n)$, λ_j is the Lagrange multiplier [51,52,54–56]. It should be noted here that the quantum system has a finite energy bandwidth, which means the effective coupling strength $\Omega_{\text{eff}}/2$ should have an upper bound value, there would be a constraint which related to the Hilbert-Schmidt. i.e., $f_0(\hat{H}_{\text{eff}}) = [\text{Tr}(\hat{H}^2_{\text{eff}}) - \Omega^2_{\text{eff}}]/2 = 0$. On the other hand, we can get the phase $\phi_1(t) = 2(\gamma - \pi)t/\tau$ and the corresponding minimum gate time $\tau = 2\sqrt{\pi^2 - (\pi - \gamma)^2}/\Omega_{\text{eff}}$ [52,54,56,76] by solving Eq. (10). (The process is shown in Appendix C.) Additionally, the evolution time decreases as the geometric phase γ decreases, when γ is equal to π, the gate time is $2\pi/\Omega_{\text{eff}}$, which is consistent with the gate time of the conventional NHQC scheme. After the TOC technique is applied to our controlled two-qubit model, the arbitrary robust quantum gates can be obtained and the numerical results are presented in the next section.

IV. NUMERICAL SIMULATIONS AND DISCUSSIONS

A. Parameter considerations and numerical methods

In this section, we introduce the details of numerical methods and gate parameters. In 5.2 μK, the lifetime of $|r\rangle_c$ and $|u\rangle_c$ is about 1900 μs and 638 μs, with thecorresponding decay rate 0.53 kHz and 1.57 kHz, respectively. The lifetime of $|r\rangle_t$ and $|\nu\rangle_t$ is about 1400 μs and 548 μs, with thecorresponding decay rate 0.71 kHz and 1.82 kHz, respectively [69]. Other parameters are $\Omega_c = \Omega_b = 2\pi \times 4.6$ MHz and $\Delta = 2\pi \times 290$ MHz. Specifically, the dipole-dipole interaction is $B = 2\pi \times 25$ MHz with an atomic distance 3.98 μm, which can be implemented in experiments [77,78].

The evolution of the quantum system under noises is governed by the Lindblad equation

$$\dot{\rho}(t) = i[\rho(t), \hat{H}(t)] + \sum_{m=1}^{4} \hat{\mathcal{L}}_m(\rho), \quad (11)$$

where $\rho(t)$ is the density matrix of the quantum system and the

$$\hat{\mathcal{L}}_1(\rho) = \sum_{k=r_c,u_c} \sum_{j=0,1} L^c_{jk}\rho L^{c\,\dagger}_{jk} - \frac{1}{2}\{L^{c\,\dagger}_{jk} L^c_{jk}, \rho\},$$

$$\hat{\mathcal{L}}_2(\rho) = \sum_{k=r_t,\nu_t} \sum_{j=0,1} L^t_{jk}\rho L^{t\,\dagger}_{jk} - \frac{1}{2}\{L^{t\,\dagger}_{jk} L^t_{jk}, \rho\},$$

$$\hat{\mathcal{L}}_3(\rho) = \sum_{k=r_c,u_c} L^c_k\rho L^{c\,\dagger}_k - \frac{1}{2}\{L^{c\,\dagger}_k L^c_k, \rho\},$$

$$\hat{\mathcal{L}}_4(\rho) = \sum_{k=r_t,\nu_t} L^t_k\rho L^{t\,\dagger}_k - \frac{1}{2}\{L^{t\,\dagger}_k L^t_k, \rho\},$$

are the Lindbladian operators, where c, t represent the control and target atoms, respectively, and $L^{c,t}_{j,k} = \sqrt{\Gamma_k}|j\rangle_\alpha\langle k|$, $L^{c,t}_k = \sqrt{\Gamma^z_k}(|k\rangle_\alpha\langle k| - |0\rangle_\alpha\langle 0| - |1\rangle_\alpha\langle 1|)$ $(\alpha = c, t)$, Γ_k describes the spontaneous emission rate of Rydberg states to the ground states and Γ^z_k represents the dephasing rate. $\hat{H}(t)$ is the three-step time-dependent Hamiltonian and we define the form of two-qubit controlled gates as

$$\text{C-}T \equiv |1\rangle\langle 1| \otimes T + |0\rangle\langle 0| \otimes I,$$
$$\text{C-}\sqrt{H} \equiv |1\rangle\langle 1| \otimes \sqrt{H} + |0\rangle\langle 0| \otimes I, \quad (12)$$

where $T = \begin{pmatrix} 1 & 0 \\ 0 & e^{i\pi/4} \end{pmatrix}$ and $H = \frac{1}{\sqrt{2}}\begin{pmatrix} 1 & 1 \\ 1 & -1 \end{pmatrix} = \sqrt{H}\cdot\sqrt{H}$, the standard single qubit $\pi/8$ gate and Hadamard gate, respectively. To realize C-T and C-$\sqrt{H}$ gates, the parameters are respectively chosen as

$$\theta = 0, \quad \phi = 0, \quad \gamma = \pi/4 \quad \text{for C-}T,$$
$$\theta = \pi/4, \quad \phi = \pi, \quad \gamma = \pi/2 \quad \text{for C-}\sqrt{H}. \quad (13)$$

To demonstrate the efficiency and robustness of our proposal under various initial conditions, the average fidelity is adopted [79,80]

$$\bar{F}(\epsilon, \hat{U}) = \frac{\sum_j \text{tr}[\hat{U}\hat{U}_j^\dagger U^\dagger \epsilon(\hat{U}_j)] + d_j^2}{d_j^2(d_j + 1)}, \quad (14)$$

where $\hat{U}_j$ is the tensor of Pauli matrices $\hat{I}\hat{I}$, $\hat{I}\hat{\sigma}_x$, ..., $\hat{\sigma}_z\hat{\sigma}_z$. $\hat{U}$ is the ideal two-qubit controlled gate defined in Eq. (9), $d_j = 4$ for a two-qubit gate, and $\epsilon(\hat{U}_j)$ is the trace-preserving quantum operation obtained by solving the master equation (11).

B. Gate performance

First, we numerically simulate the evolution paths of C-T gate and C-$\sqrt{H}$ gate of TONHQC and conventional NHQC schemes on the Bloch sphere as shown in Fig. 3, shorter paths than NHQC can be achieved to minimize the influence of

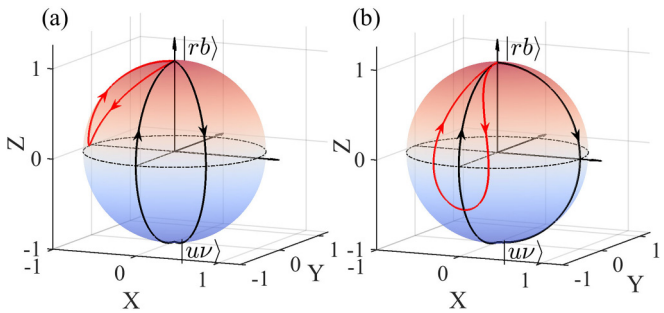

FIG. 3. Geometric illustration of the proposed TONHQC gate on the Bloch sphere, where the state $|rb\rangle$ undergoes a cyclic evolution following the red path. However, the conventional NHQC takes a cyclic evolution following the longer black path. Evolution path in these two schemes of C-T gate in (a) and C-$\sqrt{H}$ gate in (b).

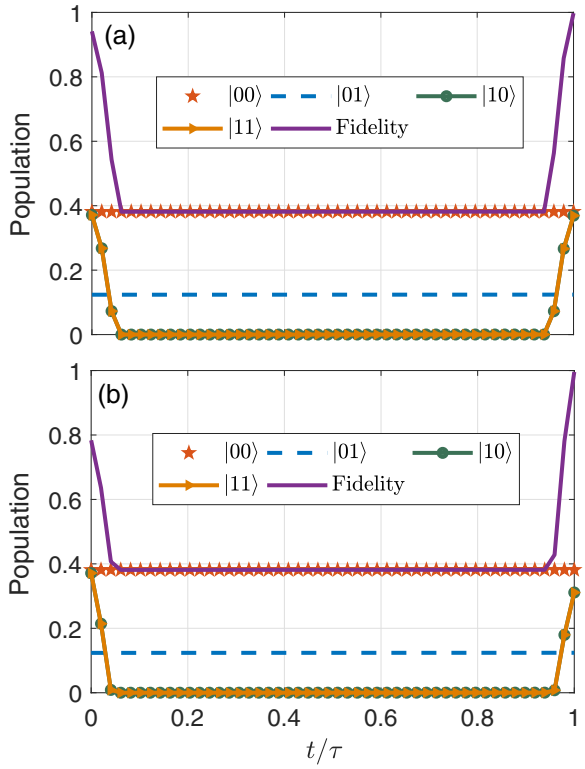

FIG. 4. The dynamics of the quantum system based on our three-step scheme. The average fidelity (purple line) of C-T gate in (a) and C-$\sqrt{H}$ in (b). The population of $|00\rangle$ (pentagrams), $|01\rangle$ (blue line), $|10\rangle$ (green line), $|11\rangle$ (yellow line) for C-T gate in (a) and C-$\sqrt{H}$ gate in (b).

environmental decoherence. The gate fidelity of C-T, C-$\sqrt{H}$ and the evolution of $\{|00\rangle, |01\rangle, |10\rangle, |11\rangle\}$ state varying with time are shown in Fig. 4, where the population of $|00\rangle$ and $|01\rangle$ is always the same and constant, and the population of $|10\rangle$ and $|11\rangle$ is 0 during the second step because the control atom is excited to the Rydberg state. The final fidelity for C-T and C-$\sqrt{H}$ are 0.9976 and 0.9962, respectively.

Next, lasers have inevitable phase noise leading to the dephasing of Rabi oscillation, which can be described by the Lindblad equation with Lindbladian operator $\hat{\mathcal{L}}_l^{\alpha}(\rho) = \hat{L}_l^{\alpha}\rho\hat{L}_l^{\alpha\dagger} - \frac{1}{2}\{\hat{L}_l^{\alpha\dagger}\hat{L}_l^{\alpha}, \rho\}$ ($\alpha = \mathrm{c}, \mathrm{t}$, represents control and target atoms, respectively), where $\hat{L}_l^{\mathrm{c}} = \sqrt{\kappa/2}(|r\rangle_{\mathrm{c}}\langle r| - |1\rangle_{\mathrm{c}}\langle 1|)$, $\hat{L}_l^{\mathrm{t}} = \sqrt{\kappa/2}(|r\rangle_{\mathrm{t}}\langle r| - |b\rangle_{\mathrm{t}}\langle b|)$ [6,81–84] and we set the dephasing rate $\kappa/2\pi \leqslant 0.1$ MHz for both control and target atoms [5]. The numerical results for laser phase noise are shown in Fig. 5. We find the fidelity is still higher than 0.85 even though the decay rate of laser phase noise approaches 0.1 MHz, where the strength of laser phase noise is larger than the current experimental condition [78]. So the high-fidelity of quantum gates can be realized even though there exist external noises based on our proposal.

In addition, we simulate the dynamics of the quantum system with noises of the Doppler shift. The dephasing of the Rydberg atom is neglected due to it can be efficiently suppressed [10,85]. The destructive effect of Doppler shift can be described by a random phase change $k_{\mathrm{eff}}v_z t$, where $k_{\mathrm{eff}} = 7.63 \times 10^6\ \mathrm{m}^{-1}$ is the effective wave vector of the laser beam

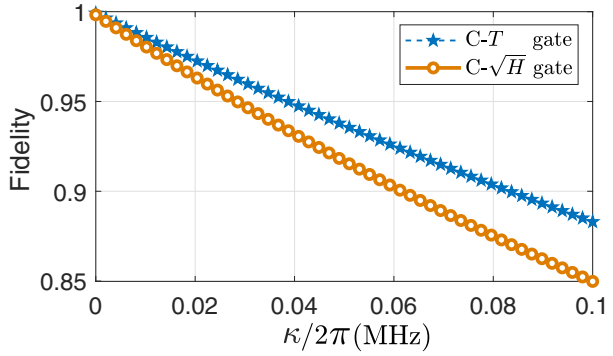

FIG. 5. The average gate fidelities with laser phase noise. Pentagrams (circle) represent the fidelity of C-T (C-$\sqrt{H}$) gate versus dephasing rate κ.

[29], and the velocity v_z of each atom is Gaussian distributed with variance $\sigma_{v_z} = \sqrt{k_B T_a/m}$. k_B is the Boltzmann constant, T_a the atomic temperature, and m the atomic mass. The numerical results of fidelities for both C-T gate and C-$\sqrt{H}$ gate under Doppler shift caused by finite temperature are shown in Fig. 6. Here the simulation of temperature is much higher than the current experimental condition, and it should be pointed out that the temperature of atoms in a tweezer can be cooled to 5.2 μK [83]. So, the fidelity of quantum gates is still higher than 95% even though there is a Doppler shift.

C. Discussion

Based on the expressions of τ, it can be found that the fluctuations with Ω_{eff} [31,86] would induce the ideal time variant. Here, we consider that the deviation of time from the ideal case can be expressed as a Taylor expansion

$$\tau' = \frac{2\sqrt{\pi^2 - (\pi - \gamma)^2}}{\Omega_{\mathrm{eff}}(1+\eta)} \simeq \tau - \eta\tau + \eta^2\tau - \eta^3\tau. \tag{15}$$

When the fluctuation $\eta = 0.05 \ll 1$, $\tau' \simeq 0.952\tau$ after omitting the high-order terms. However, we still follow the gate time τ in the actual experiment, so the simplest way to consider the possible deviation of QBE's solution is to discuss

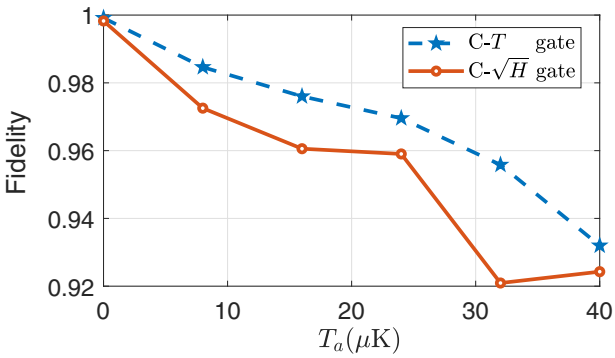

FIG. 6. The average gate fidelities at different temperatures T_a. Pentagrams (circle) represent the fidelity of C-T (C-$\sqrt{H}$) gate versus $T_a \in [0, 40]$ μK.

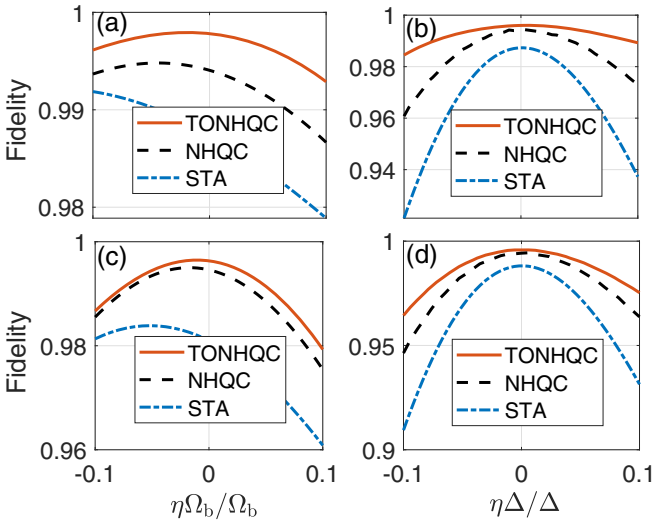

FIG. 7. Robustness of quantum gates (a), (b) C-T and (c), (d) C-$\sqrt{H}$ against (a), (c) the Rabi frequency fluctuation $\eta\Omega_b/\Omega_b \in [-0.1, 0.1]$ and (b), (d) detuning fluctuation $\eta\Delta/\Delta \in [-0.1, 0.1]$. The red line represents the time-optimal-control NHQC (TONHQC), the black line represents the conventional NHQC and the blue line represents the shortcuts to adiabaticity (STA).

the fluctuations related to Ω_{eff}, i.e., Rabi frequencies Ω_b and the detuning Δ of optical excitation. To demonstrate the robustness of our proposal, we simulate the dynamics of the quantum system with the noises, including Rabi frequency fluctuation, detuning fluctuation, and spontaneous emission of atoms compared with NHQC and shortcuts to the adiabaticity (STA) scheme (see Appendix D for details). The numerical results of Rabi frequency fluctuation and detuning fluctuation are shown in Fig. 7. The fidelity of the two quantum gates for the TONHQC is $\gtrsim$99% in the range of 10% fluctuations, while the fidelity for the conventional NHQC and STA dramatically decreases as the strength of fluctuation increases. We find the results for our proposal are more robust than the others. In addition, we list the gate times for three schemes with the same $\Omega_{\max} = \Omega_{\text{eff}} = 2\pi \times 0.4$ MHz, which are shown in Table I. It should be pointed out that the required time of STA has no advantage in contrast to TONHQC for this scheme, and this is accurately the reason why the performance is not better than TONHQC.

The quantum simulations of spontaneous emission of the Rydberg state are shown in Fig. 8. We plot the fidelities for C-T and C-$\sqrt{H}$ gates as a function of decay rate Γ for three schemes. In Fig. 8, we assume that all Γ_k are equal and denoted by Γ for simplicity, and set $\Gamma_0 = 1.5$ kHz and $\Gamma/\Gamma_0 \in [0.1, 20]$. The numerical simulation highlights the

TABLE I. Gate time τ (μs) for three schemes with the same $\Omega_{\max}$.

	Gate	
Scheme	C-T	C-$\sqrt{H}$
TONHQC	1.88	2.4
Conventional NHQC	2.74	2.74
STA	5.6	5.6

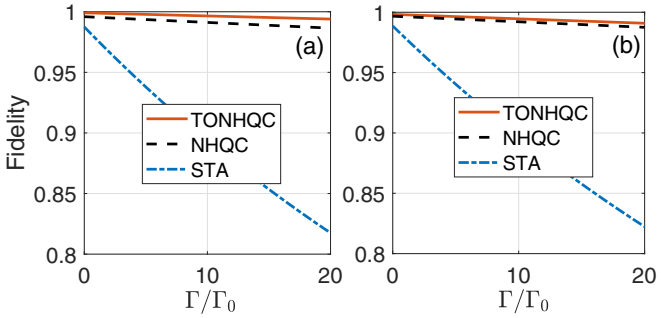

FIG. 8. Robustness of quantum gates (a) C-T and (b) C-$\sqrt{H}$ against the decay rate. The red line represents the TONHQC, the black line represents NHQC, and the blue line represents the STA.

robustness of our proposal compared with the previous scheme under spontaneous emission. Above all, we can find that TONHQC has a better higher fidelity and better robustness for $\gamma < \pi$, the smaller γ is, the better the performance. Compared to NHQC, the TONHQC scheme does not need to meet the dynamical phase always to be 0 as conventional NHQC does, and it has better robustness compared to the other two schemes.

V. CONCLUSION

In conclusion, we propose a universal time-optimal nonadiabatic holonomic two-qubit controlled-gate scheme realized by three-step operations. High-fidelity quantum gates are realized in the Rydberg atoms model. The efficiency and robustness of our proposal are demonstrated by the numerical simulations comparing our proposal with the conventional NHQC and STA under several kinds of noises, including the Rabi error, detuning error, laser phase noise, Doppler shift, and spontaneous emission. Furthermore, our scheme is expected to be able to provide a promising method for the implementation of multiple-qubit controlled gates in Rydberg atoms and may pave the way to realize fault-tolerant quantum computation in the future.

ACKNOWLEDGMENTS

We would like to thank Dr. F.-Q. Guo for the helpful discussions. This work was supported by the National Key R & D Program of China (Grants No. 2022YFA1404500 and No. 2021YFA1400900); the National Natural Science Foundation of China under Grants No. 12274376, No. 12204424, No. 12204428, and No. 12074346; the Major Science and Technology project of Henan Province under Grant No. 221100210400; the Natural Science Foundation of Henan Province under Grant No. 212300410085; the Cross-Disciplinary Innovative Research Group Project of Henan Province under Grant No. 232300421004.

APPENDIX A: SINGLE-QUBIT GATE WITH TOC

Due to the inadequacy to demonstrate universality by only implementing controlled arbitrary two-qubit gates, we here construct single-qubit gate on the target atom to expound universality. When we simply set $\Delta = 0$, the Hamiltonian on the target atom is

$$\hat{H}_t = \tfrac{1}{2}\Omega_b e^{-i\phi_1(t)}|r\rangle\langle b| + \text{H.c.} \tag{A1}$$

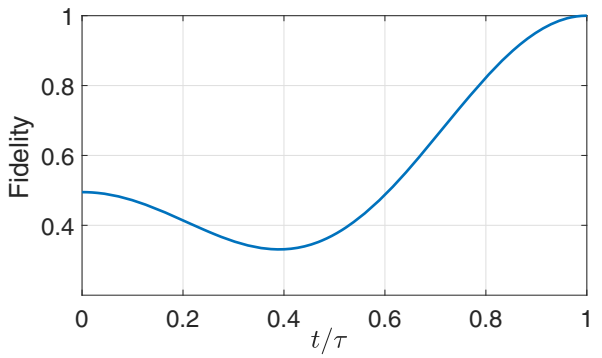

FIG. 9. Gate fidelity of X gate for average dynamics with TONHQC.

The evolution operator $\hat{U}(\tau)$ can be calculated as

$$\hat{U}(\tau) = e^{i\gamma}|b\rangle\langle b| + |d\rangle\langle d|, \tag{A2}$$

and can be spanned in the logical qubit subspace $\{|0\rangle, |1\rangle\}$ as

$$e^{i\frac{\gamma}{2}}\begin{pmatrix} \cos\frac{\gamma}{2} - i\cos\theta\sin\frac{\gamma}{2} & ie^{i\phi}\sin\frac{\gamma}{2}\sin\theta \\ ie^{-i\phi}\sin\frac{\gamma}{2}\sin\theta & \cos\frac{\gamma}{2} + i\cos\theta\sin\frac{\gamma}{2} \end{pmatrix}, \tag{A3}$$

based on which one can realize universal single-qubit operations. For instance, if we want to realize the X gate, the parameters should be chosen as $\theta = \pi/2, \phi = \pi$, and $\gamma = \pi$. Then we simulate the average fidelity of the single-qubit X gate as shown in Fig. 9. Note that the single-qubit gate here is also arbitrary to satisfy the universality of single-qubit gates. In the main text, we also present arbitrary two-qubit holonomic gates, ensuring its universality to perform any quantum computing task.

APPENDIX B: ROBUST PROPERTIES OF GEOMETRIC PHASE μ_a

In Sec. III in the main text, we show $G_{lk} = G^{\mu}_{lk} + G^{\xi}_{lk}$, where $G^{\mu}_{lk} = \sum_a i\langle\Psi_l(t)|\partial/\partial\mu|\Psi_k(t)\rangle(d\mu_a/dt)$, and $G^{\xi}_{lk} = \sum_b i\langle\Psi_l(t)|\partial/\partial\xi|\Psi_k(t)\rangle(d\xi_b/dt)$. Below, we briefly describe the elimination of the dynamical part and the remaining pure geometric part of holonomic gates in our scheme. Due to

$$\begin{aligned} G^{\xi}_{lk} &= \sum_b i\langle\Psi_l(t)|\partial/\partial\xi|\Psi_k(t)\rangle(d\xi_b/dt) \\ &= ie^{i\mu_a(t)}\langle\Psi_l(t)|\partial/\partial\xi|\psi_k[\xi_b(t)]\rangle \\ &= e^{i\mu_a(t)}\langle\Psi_l(t)|i|\dot{\psi}_k[\xi_b(t)]\rangle, \end{aligned} \tag{B1}$$

and the dynamical part of the above evolution operator $\hat{U}(\tau)$ can be giving rise to

$$\begin{aligned} D_{lk} &= -\langle\Psi_l(t)|\hat{H}(t)|\Psi_k(t)\rangle \\ &= -i\langle\Psi_l(t)|\hat{H}(t)e^{i\mu_a(t)}|\psi_k(t)\rangle \\ &= -ie^{i\mu_a(t)}\langle\Psi_l(t)|\hat{H}(t)|\psi_k[\xi_b(t)]\rangle \\ &= -e^{i\mu_a(t)}\langle\Psi_l(t)|i|\dot{\psi}_k[\xi_b(t)]\rangle. \end{aligned} \tag{B2}$$

So, it can be concluded that the dynamical part is partially offset by the geometric part G_{lk}, i.e., $D_{lk} + G^{\xi}_{lk} = 0$. A new state vector can be defined as $|\tilde{\Psi}(\mu_a, \xi_b)\rangle = e^{i\int f_a(t)dt}|\psi_a(\mu_a, \xi_b)\rangle$, where $|\psi_a(\mu_a, \xi_b)\rangle = e^{i\mu_a}|\psi_a(\xi_b)\rangle$ satisfies the Schrödinger equation and $f_a(t) = \langle\psi_a(\mu_a, \xi_b)|\hat{H}|\psi_a(\mu_a, \xi_b)\rangle$ is used to counteract the dynamical phase [87]. Then we find

$$\begin{aligned} &\langle\tilde{\Psi}_a(\mu_a, \xi_b)|id/dt|\tilde{\Psi}_a(\mu_a, \xi_b)\rangle \\ &= -\langle\psi_a(\mu_a, \xi_b)|\hat{H}|\psi_a(\mu_a, \xi_b)\rangle \\ &\quad +\langle\psi_a(\mu_a, \xi_b)|id/dt|\psi_a(\mu_a, \xi_b)\rangle \\ &= -f_a(t) + \langle\psi_a(\mu_a, \xi_b)|\hat{H}|\psi_a(\mu_a, \xi_b)\rangle \\ &= 0. \end{aligned} \tag{B3}$$

The expression dependent on μ_a is given by

$$i\langle\tilde{\Psi}_a(\mu_a, \xi_b)|\partial/\partial\xi_b|\tilde{\Psi}(\mu_a, \xi_b)\rangle d\xi_b/dt + \dot{\mu}_a = 0. \tag{B4}$$

Finally, we obtain

$$\mu_a = -i\oint\langle\psi_a(\xi_b)|d/d\xi_b|\psi_a(\xi_b)\rangle d\xi_b. \tag{B5}$$

Thus, the geometric phase μ_a is independent of the Hamiltonian and only depends on the Hilbert space structure. In addition, the diagonal gate operator $\hat{U}(\tau) = \sum_a e^{i\mu_a(\tau)}|\Psi_a(0)\rangle\langle\Psi_a(0)|$ satisfies the gauge invariance that verifies the geometric property of holonomic gates.

APPENDIX C: ANALYTIC SOLUTION OF QBE

According to the authors of Ref. [51], we first provide the time functional required to transition from one state to another in quantum space, to find a suitable state and Hamiltonian to optimize it. The time functional is given as follows:

$$\begin{aligned} S[\psi, \hat{H}, \phi, \lambda] = &\underbrace{\int \frac{\sqrt{\langle\partial_t\psi|(I-P)|\partial_t\psi\rangle}}{\Delta E}}_{\text{(I)}} \\ &+ \underbrace{(-i\langle\phi|\partial_t\psi\rangle + \langle\phi|\hat{H}|\psi\rangle}_{\text{(II)}} \\ &- \underbrace{i\langle\psi|\hat{H}|\phi\rangle + \langle\psi|\hat{H}|\phi\rangle)}_{\text{(III)}} \\ &+ \underbrace{\lambda_1[\mathrm{Tr}(\hat{\hat{H}})/2 - \omega^2] + \sum_{j=2}^{m}\lambda_j f_j(\hat{H})dt}_{\text{(IV)}}, \end{aligned} \tag{C1}$$

where ϕ and λ are Lagrange multipliers, $P = |\psi\rangle\langle\psi|$, $\partial_t = d/dt$, I is the unit operator, and $\Delta E = \sqrt{\langle\hat{H}^2\rangle - \langle\hat{H}\rangle^2}$ is defined as variance, ω is a constant which can be interpreted as the energy uncertainty associated with the transition. It is worth noting that $\hat{H}$ here refers to $\hat{H}_{\text{eff}}$ in the main text. Necessarily, we explain the meanings of the four terms, which together form the constraints of the functional.

$\sqrt{\langle\partial_t\psi|(I-P)|\partial_t\psi\rangle}$ in (I) represents the quantity ds in a quantum mechanical term and it is the quantum line element on the space in which quantum states live, which can be measured by the Fubini-Study metric [88,89].

(II) and (III) represent the constraint imposed on a quantum state, that is, the Schrödinger equation always needs to be satisfied. Comprehensively, we consider both the contribution

of Schrödinger equation and its Hermitian conjugate to the action.

The first term in (IV) represents that we take the constraint that the energy uncertainty ΔE is bounded by using Lagrangian multipliers and it can be limited by selecting the appropriate Hamiltonian $\hat{H}$. The second term denotes some specific experimental conditions that may exist that limit the Hamiltonian operators acting on quantum states.

In line with Ref. [51], we perform the variation of all variables in Eq. (C1) and obtain

$$0 = (\dot{\hat{F}} + i[\hat{H}, \hat{F}])|\psi\rangle, \tag{C2}$$

where the operator $\hat{F}$ involves the constraint functions $f_j(H)$ and is given by

$$\hat{F} = \sum_{j=1}^{M} \lambda_j \partial_H f_j(\hat{H}). \tag{C3}$$

Particularly, Eq. (C2) indicates that $\hat{F}|\psi\rangle$ satisfies the Schrödinger equation, which leads to

$$\dot{\hat{F}} = -i[\hat{H}, \hat{F}]. \tag{C4}$$

According to the solution of Ref. [90], and consider the initial state $|\psi(0)\rangle = |rb\rangle = \binom{1}{0}$, $\hat{\tilde{H}}(0)$ can be expressed as $\begin{pmatrix} 0 & \omega(\cos\phi - i\sin\phi) \\ \omega(\cos\phi + i\sin\phi) & 0 \end{pmatrix}$. Thus, $\hat{H}(t) = \hat{\tilde{H}}(t) = e^{i(\Omega\hat{\sigma}_z)t}\hat{\tilde{H}}(0)e^{-i(\Omega\hat{\sigma}_z)t} = \begin{pmatrix} 0 & \omega e^{-i(\phi_0 - 2\Omega t)} \\ \omega e^{i(\phi_0 - 2\Omega t)} & 0 \end{pmatrix} = \omega\cos\phi_1(t)\hat{\sigma}_x + \omega\sin\phi_1(t)\hat{\sigma}_y$, where $\phi_1(t) = -2\Omega t + \phi_0$, in which $\Omega = \lambda_2/\lambda_1$, and $\hat{\sigma}_x$, $\hat{\sigma}_y$ are Pauli operators under the basis $\{|rb\rangle, |uv\rangle\}$. Based on the target evolution operator $\hat{U}_F = R(\hat{z}, \theta')$, $\theta' \in (0, 2\pi)$, i.e., Eq. (8) in the main text, we can derive

$$\tau = \frac{2\sqrt{\pi^2 - (\pi - \gamma)^2}}{\Omega_{\text{eff}}}, \tag{C5}$$

$$\phi_1(t) = 2(\gamma - \pi)/\tau. \tag{C6}$$

This result is consistent with the result in Ref. [56] when $\delta = 0$, $\theta' = -2\gamma$, $\Omega = (-2\pi + \theta)/2\tau$.

APPENDIX D: SCHEME BASED ON SHORTCUTS TO ADIABATICITY

The shortcuts to adiabaticity (STA) technique has been developed rapidly [91–94], which also has made it a popularly optimized method. To demonstrate the superiority of our scheme, we provide a comparison between the STA based on Lewis-Riesenfeld (LR) invariant method [49,67,95,96] and our proposed TOC scheme as well as conventional NHQC here. According to Eq. (6) satisfing the Schrödinger equation $i\partial_t|\psi_k(t)\rangle = \hat{H}_{\text{eff}}|\psi_k(t)\rangle$, we inversely engineer the driving Hamiltonian [97]. $|\psi_k(t)\rangle$ in the subspace $\{|rb\rangle, |uv\rangle\}$ could be parameterized as

$$|\psi_k(t)\rangle = e^{-i\chi(t)/2}\begin{pmatrix} \cos\frac{\Theta(t)}{2}e^{-i\beta(t)/2} \\ \sin\frac{\Theta(t)}{2}e^{i\beta(t)/2} \end{pmatrix}, \tag{D1}$$

in which $\Theta(t)$, $\beta(t)$ are two time-dependent angles and $\chi(t)$ is a parameterized phase. To make the initial state of the system cyclically evolved along the $|\psi_k(t)\rangle$ under the driving of the

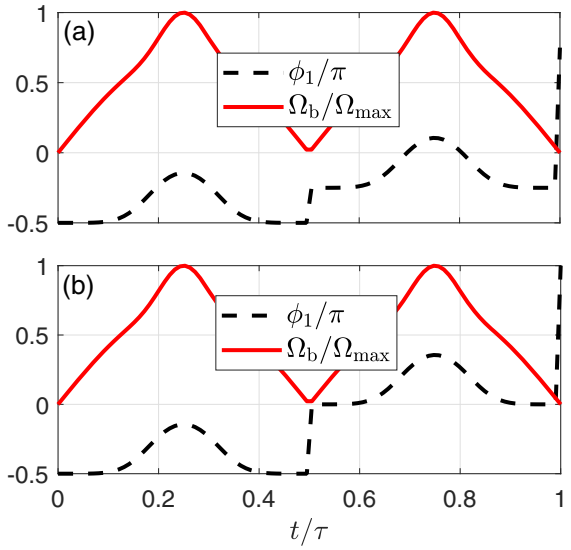

FIG. 10. The Rabi frequency Ω_b (solid red line) and ϕ_1 (black dashed line) versus t/τ of STA for the (a) C-T gate and (b) C-$\sqrt{H}$ gate, respectively, in which $\Omega_{max} = 2\pi \times 0.4$ MHz and $\tau = 5.6$ μs.

$\hat{H}_{\text{eff}}$, we can choose a suitable set of parameters $\beta(t)$ and $\Theta(t)$ inversely to derive $\Omega_b(t)$ and $\phi_1(t)$ following as

$$\begin{aligned} \phi_1(t) &= \arctan[\dot{\Theta}(t)\cot\Theta/\dot{\beta}(t)] - \beta(t), \\ \Omega_b(t) &= -\dot{\Theta}(t)/\sin[\beta(t) + \phi_1(t)]. \end{aligned} \tag{D2}$$

Specifically, we use the shape of $\Omega_b(t)$ in Eq. (D2) shown in Fig. 10 with $\Omega_{max} = \Omega_{\text{eff}} = 2\pi \times 0.4$ MHz. To achieve a cyclic evolution, a simple choice is setting $\Theta(t) = \pi\sin^2(\pi t/\tau)$ to satisfy the boundary conditions $\beta(0) = \beta(\tau) = 0$, where τ is the total evolution time and $\tau = 5.6$ μs for both C-T gate and C-$\sqrt{H}$ gate. In addition, to satisfy the condition $\int_0^\tau \langle\psi_k(t)|\hat{H}_{\text{eff}}|\psi_k(t)\rangle dt = 0$, we set

$$\chi(t) = [2\Theta(t) - \sin(2\Theta(t))]/4, \quad t \in [0, \tau], \tag{D3}$$

$$\beta(t) = \begin{cases} -\int \dot{\chi}(t)\cos\Theta(t)dt, & t \in [0, \tau/2], \\ -\int \dot{\chi}(t)\cos\Theta(t)dt - \gamma, & t \in (\tau/2, \tau]. \end{cases} \tag{D4}$$

From the above, we can obtain the same evolution operator as Eq. (9). The evolution paths of C-T and C-$\sqrt{H}$ gates are shown in Fig. 11. According to the evolution paths of STA scheme, we can find that the gate time of STA is not short.

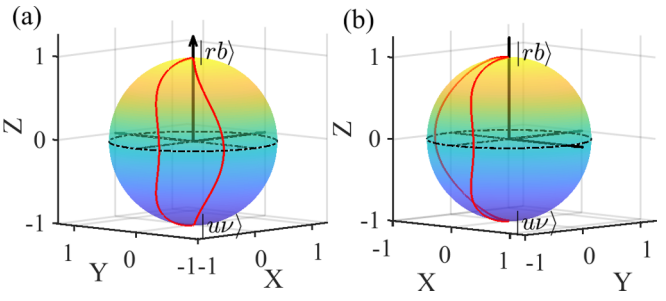

FIG. 11. Geometric illustration of the STA gate on the Bloch sphere, where the state $|rb\rangle$ undergoes a cyclic evolution following the red path. Evolution path of C-T gate in (a) and C-$\sqrt{H}$ gate in (b).

[1] P. W. Shor, Algorithms for quantum computation: discrete logarithms and factoring, *Proceedings of the 35th Annual Symposium on Foundations of Computer Science* (IEEE, New York, 1994).

[2] P. Zanardi and M. Rasetti, Holonomic quantum computation, Phys. Lett. A **264**, 94 (1999).

[3] Y. Aharonov and J. Anandan, Phase change during a cyclic quantum evolution, Phys. Rev. Lett. **58**, 1593 (1987).

[4] F. Wilczek and A. Zee, Appearance of gauge structure in simple dynamical systems, Phys. Rev. Lett. **52**, 2111 (1984).

[5] X. X. Li, X. Q. Shao, and W. Li, Single temporal-pulse-modulated parameterized controlled-phase gate for Rydberg atoms, Phys. Rev. Appl. **18**, 044042 (2022).

[6] S. de Léséleuc, D. Barredo, V. Lienhard, A. Browaeys, and T. Lahaye, Analysis of imperfections in the coherent optical excitation of single atoms to Rydberg states, Phys. Rev. A **97**, 053803 (2018).

[7] H. Tamura, T. Yamakoshi, and K. Nakagawa, Analysis of coherent dynamics of a Rydberg-atom quantum simulator, Phys. Rev. A **101**, 043421 (2020).

[8] J. Anandan, Non-adiabatic non-abelian geometric phase, Phys. Lett. A **133**, 171 (1988).

[9] E. Sjöqvist, D. M. Tong, L. M. Andersson, B. Hessmo, M. Johansson, and K. Singh, Non-adiabatic holonomic quantum computation, New J. Phys. **14**, 103035 (2012).

[10] G. F. Xu, J. Zhang, D. M. Tong, E. Sjöqvist, and L. C. Kwek, Nonadiabatic holonomic quantum computation in decoherence-free subspaces, Phys. Rev. Lett. **109**, 170501 (2012).

[11] M. V. Berry, Quantal phase factors accompanying adiabatic changes, Proc. R. Soc. London A **392**, 45 (1984).

[12] B.-J. Liu, L.-L. Yan, Y. Zhang, M.-H. Yung, S.-L. Su, and C. X. Shan, Decoherence-suppressed nonadiabatic holonomic quantum computation, Phys. Rev. Res. **5**, 013059 (2023).

[13] K. Nagata, K. Kuramitani, Y. Sekiguchi, and H. Kosaka, Universal holonomic quantum gates over geometric spin qubits with polarised microwaves, Nat. Commun. **9**, 3227 (2018).

[14] S. Arroyo-Camejo, A. Lazariev, S. W. Hell, and G. Balasubramanian, Room temperature high-fidelity holonomic single-qubit gate on a solid-state spin, Nat. Commun. **5**, 4870 (2014).

[15] Y. Sekiguchi, N. Niikura, R. Kuroiwa, H. Kano, and H. Kosaka, Optical holonomic single quantum gates with a geometric spin under a zero field, Nat. Photon. **11**, 309 (2017).

[16] B. B. Zhou, P. C. Jerger, V. O. Shkolnikov, F. J. Heremans, G. Burkard, and D. D. Awschalom, Holonomic quantum control by coherent optical excitation in diamond, Phys. Rev. Lett. **119**, 140503 (2017).

[17] N. Ishida, T. Nakamura, T. Tanaka, S. Mishima, H. Kano, R. Kuroiwa, Y. Sekiguchi, and H. Kosaka, Universal holonomic single quantum gates over a geometric spin with phase-modulated polarized light, Opt. Lett. **43**, 2380 (2018).

[18] M.-Z. Ai, S. Li, Z. Hou, R. He, Z.-H. Qian, Z.-Y. Xue, J.-M. Cui, Y.-F. Huang, C.-F. Li, and G.-C. Guo, Experimental realization of nonadiabatic holonomic single-qubit quantum gates with optimal control in a trapped ion, Phys. Rev. Appl. **14**, 054062 (2020).

[19] G. Feng, G. Xu, and G. Long, Experimental realization of nonadiabatic holonomic quantum computation, Phys. Rev. Lett. **110**, 190501 (2013).

[20] Z. Zhu, T. Chen, X. Yang, J. Bian, Z.-Y. Xue, and X. Peng, Single-loop and composite-loop realization of nonadiabatic holonomic quantum gates in a decoherence-free subspace, Phys. Rev. Appl. **12**, 024024 (2019).

[21] H. Li, Y. Liu, and G. L. Long, Experimental realization of single-shot nonadiabatic holonomic gates in nuclear spins, Sci. China Phys. Mech. Astron. **60**, 080311 (2017).

[22] S. Danilin, A. Vepsäläinen, and G. S. Paraoanu, Experimental state control by fast non-abelian holonomic gates with a superconducting qutrit, Phys. Scr. **93**, 055101 (2018).

[23] D. J. Egger, M. Ganzhorn, G. Salis, A. Fuhrer, P. Müller, P. Kl. Barkoutsos, N. Moll, I. Tavernelli, and S. Filipp, Entanglement generation in superconducting qubits using holonomic operations, Phys. Rev. Appl. **11**, 014017 (2019).

[24] C. Song, S.-B. Zheng, P. Zhang, K. Xu, L. Zhang, Q. Guo, W. Liu, D. Xu, H. Deng, K. Huang, D. Zheng, X. Zhu, and H. Wang, Continuous-variable geometric phase and its manipulation for quantum computation in a superconducting circuit, Nat. Commun. **8**, 1061 (2017).

[25] M. Saffman, T. G. Walker, and K. Mølmer, Quantum information with Rydberg atoms, Rev. Mod. Phys. **82**, 2313 (2010).

[26] D. S. Weiss and M. Saffman, Quantum computing with neutral atoms, Phys. Today **70**, 44 (2017).

[27] C. S. Adams, J. D. Pritchard, and J. P. Shaffer, Rydberg atom quantum technologies, J. Phys. B: At. Mol. Opt. Phys. **53**, 012002 (2019).

[28] M. Saffman, I. I. Beterov, A. Dalal, E. J. Páez, and B. C. Sanders, Symmetric Rydberg controlled-z gates with adiabatic pulses, Phys. Rev. A **101**, 062309 (2020).

[29] F. Robicheaux, T. M. Graham, and M. Saffman, Photon-recoil and laser-focusing limits to Rydberg gate fidelity, Phys. Rev. A **103**, 022424 (2021).

[30] T. M. Wintermantel, Y. Wang, G. Lochead, S. Shevate, G. K. Brennen, and S. Whitlock, Unitary and nonunitary quantum cellular automata with Rydberg arrays, Phys. Rev. Lett. **124**, 070503 (2020).

[31] S. J. Evered, D. Bluvstein, M. Kalinowski, S. Ebadi, T. Manovitz, H. Zhou, S. H. Li, A. A. Geim, T. T. Wang, N. Maskara, H. Levine, G. Semeghini, M. Greiner, V. Vuletić, and M. D. Lukin, High-fidelity parallel entangling gates on a neutral-atom quantum computer, Nature (London) **622**, 268 (2023).

[32] W. Li and I. Lesanovsky, Entangling quantum gate in trapped ions via Rydberg blockade, Appl. Phys. B **114**, 37 (2014).

[33] D. Comparat and P. Pillet, Dipole blockade in a cold Rydberg atomic sample, J. Opt. Soc. Am. B **27**, A208 (2010).

[34] S.-L. Su, F.-Q. Guo, L. Tian, X.-Y. Zhu, L.-L. Yan, E.-J. Liang, and M. Feng, Nondestructive Rydberg parity meter and its applications, Phys. Rev. A **101**, 012347 (2020).

[35] D. Bluvstein, A. Omran, H. Levine, A. Keesling, G. Semeghini, S. Ebadi, T. T. Wang, A. A. Michailidis, N. Maskara, W. W. Ho, S. Choi, M. Serbyn, M. Greiner, V. Vuletić, and M. D. Lukin, Controlling quantum many-body dynamics in driven Rydberg atom arrays, Science **371**, 1355 (2021).

[36] M. D. Lukin, M. Fleischhauer, R. Cote, L. M. Duan, D. Jaksch, J. I. Cirac, and P. Zoller, Dipole blockade and quantum information processing in mesoscopic atomic ensembles, Phys. Rev. Lett. **87**, 037901 (2001).

[37] D. Møller, L. B. Madsen, and K. Mølmer, Quantum gates and multiparticle entanglement by Rydberg excitation blockade and adiabatic passage, Phys. Rev. Lett. **100**, 170504 (2008).

[38] P. Scholl, A. L. Shaw, R. B.-S. Tsai, R. Finkelstein, J. Choi, and M. Endres, Erasure conversion in a high-fidelity Rydberg quantum simulator, Nature (London) **622**, 273 (2023).

[39] N. Lorenz, L. Festa, L.-M. Steinert, and C. Gross, Raman sideband cooling in optical tweezer arrays for Rydberg dressing, SciPost Phys. **10**, 052 (2021).

[40] E. Urban, T. A. Johnson, T. Henage, L. Isenhower, D. D. Yavuz, T. G. Walker, and M. Saffman, Observation of Rydberg blockade between two atoms, Nat. Phys. **5**, 110 (2009).

[41] L. Béguin, A. Vernier, R. Chicireanu, T. Lahaye, and A. Browaeys, Direct measurement of the van der Waals interaction between two Rydberg atoms, Phys. Rev. Lett. **110**, 263201 (2013).

[42] D. Jaksch, J. I. Cirac, P. Zoller, S. L. Rolston, R. Côté, and M. D. Lukin, Fast quantum gates for neutral atoms, Phys. Rev. Lett. **85**, 2208 (2000).

[43] D. Schrader, I. Dotsenko, M. Khudaverdyan, Y. Miroshnychenko, A. Rauschenbeutel, and D. Meschede, Neutral atom quantum register, Phys. Rev. Lett. **93**, 150501 (2004).

[44] S. Ma, G. Liu, P. Peng, B. Zhang, S. Jandura, J. Claes, A. P. Burgers, G. Pupillo, S. Puri, and J. D. Thompson, High-fidelity gates and mid-circuit erasure conversion in an atomic qubit, Nature (London) **622**, 279 (2023).

[45] Y. Liang, P. Shen, T. Chen, and Z.-Y. Xue, Composite short-path nonadiabatic holonomic quantum gates, Phys. Rev. Appl. **17**, 034015 (2022).

[46] F.-Q. Guo, J.-L. Wu, X.-Y. Zhu, Z. Jin, Y. Zeng, S. Zhang, L.-L. Yan, M. Feng, and S.-L. Su, Complete and nondestructive distinguishment of many-body Rydberg entanglement via robust geometric quantum operations, Phys. Rev. A **102**, 062410 (2020).

[47] C.-Y. Guo, L.-L. Yan, S. Zhang, S.-L. Su, and W. Li, Optimized geometric quantum computation with a mesoscopic ensemble of Rydberg atoms, Phys. Rev. A **102**, 042607 (2020).

[48] S.-B. Zheng, C.-P. Yang, and F. Nori, Comparison of the sensitivity to systematic errors between nonadiabatic non-abelian geometric gates and their dynamical counterparts, Phys. Rev. A **93**, 032313 (2016).

[49] Y.-H. Kang, Z.-C. Shi, B.-H. Huang, J. Song, and Y. Xia, Flexible scheme for the implementation of nonadiabatic geometric quantum computation, Phys. Rev. A **101**, 032322 (2020).

[50] Y.-H. Chen, W. Qin, R. Stassi, X. Wang, and F. Nori, Fast binomial-code holonomic quantum computation with ultrastrong light-matter coupling, Phys. Rev. Res. **3**, 033275 (2021).

[51] A. Carlini, A. Hosoya, T. Koike, and Y. Okudaira, Time-optimal quantum evolution, Phys. Rev. Lett. **96**, 060503 (2006).

[52] A. Carlini, A. Hosoya, T. Koike, and Y. Okudaira, Time-optimal unitary operations, Phys. Rev. A **75**, 042308 (2007).

[53] B.-J. Liu, Z.-Y. Xue, and M.-H. Yung, Brachistochrone nonadiabatic holonomic quantum control, arXiv:2001.05182.

[54] A. Carlini, A. Hosoya, T. Koike, and Y. Okudaira, Time optimal quantum evolution of mixed states, J. Phys. A: Math. Theor. **41**, 045303 (2008).

[55] A. Carlini and T. Koike, Time-optimal transfer of coherence, Phys. Rev. A **86**, 054302 (2012).

[56] J. Geng, Y. Wu, X. Wang, K. Xu, F. Shi, Y. Xie, X. Rong, and J. Du, Experimental time-optimal universal control of spin qubits in solids, Phys. Rev. Lett. **117**, 170501 (2016).

[57] K.-Y. Liao, X.-H. Liu, Z. Li, and Y.-X. Du, Geometric Rydberg quantum gate with shortcuts to adiabaticity, Opt. Lett. **44**, 4801 (2019).

[58] S.-L. Su, L.-N. Sun, B.-J. Liu, L.-L. Yan, M.-H. Yung, W. Li, and M. Feng, Rabi- and blockade-error-resilient all-geometric Rydberg quantum gates, Phys. Rev. Appl. **19**, 044007 (2023).

[59] J.-F. Wei, F.-Q. Guo, D.-Y. Wang, Y. Jia, L.-L. Yan, M. Feng, and S.-L. Su, Fast multiqubit Rydberg geometric fan-out gates with optimal control technology, Phys. Rev. A **105**, 042404 (2022).

[60] E. Sjöqvist, Nonadiabatic holonomic single-qubit gates in off-resonant λ systems, Phys. Lett. A **380**, 65 (2016).

[61] Y. Xu, W. Cai, Y. Ma, X. Mu, L. Hu, T. Chen, H. Wang, Y. P. Song, Z.-Y. Xue, Z.-qi Yin, and L. Sun, Single-loop realization of arbitrary nonadiabatic holonomic single-qubit quantum gates in a superconducting circuit, Phys. Rev. Lett. **121**, 110501 (2018).

[62] E. Herterich and E. Sjöqvist, Single-loop multiple-pulse nonadiabatic holonomic quantum gates, Phys. Rev. A **94**, 052310 (2016).

[63] P. Z. Zhao, G. F. Xu, Q. M. Ding, E. Sjöqvist, and D. M. Tong, Single-shot realization of nonadiabatic holonomic quantum gates in decoherence-free subspaces, Phys. Rev. A **95**, 062310 (2017).

[64] G. T. Genov, D. Schraft, N. V. Vitanov, and T. Halfmann, Arbitrarily accurate pulse sequences for robust dynamical decoupling, Phys. Rev. Lett. **118**, 133202 (2017).

[65] S. Ravets, H. Labuhn, D. Barredo, L. Béguin, T. Lahaye, and A. Browaeys, Coherent dipole–dipole coupling between two single Rydberg atoms at an electrically-tuned förster resonance, Nat. Phys. **10**, 914 (2014).

[66] S.-L. Su, E. Liang, S. Zhang, J.-J. Wen, L.-L. Sun, Z. Jin, and A.-D. Zhu, One-step implementation of the Rydberg-Rydberg-interaction gate, Phys. Rev. A **93**, 012306 (2016).

[67] H. R. Lewis, Jr. and W. B. Riesenfeld, An exact quantum theory of the time-dependent harmonic oscillator and of a charged particle in a time-dependent electromagnetic field, J. Math. Phys. **10**, 1458 (1969).

[68] I. I. Beterov and M. Saffman, Rydberg blockade, förster resonances, and quantum state measurements with different atomic species, Phys. Rev. A **92**, 042710 (2015).

[69] N. Šibalić, J. D. Pritchard, C. S. Adams, and K. J. Weatherill, Arc: An open-source library for calculating properties of alkali Rydberg atoms, Comput. Phys. Commun. **220**, 319 (2017).

[70] P. A. Kuchment, Floquet theory for partial differential equations, Russ. Math. Surv. **37**, 1 (1982).

[71] S. L. Su, H. Z. Shen, E. Liang, and S. Zhang, One-step construction of the multiple-qubit Rydberg controlled-phase gate, Phys. Rev. A **98**, 032306 (2018).

[72] A. Vepsäläinen, S. Danilin, and G. S. Paraoanu, Superadiabatic population transfer in a three-level superconducting circuit, Sci. Adv. **5**, eaau5999 (2019).

[73] A. Vepsäläinen, S. Danilin, and G. S. Paraoanu, Optimal superadiabatic population transfer and gates by dynamical phase corrections, Quantum Sci. Technol. **3**, 024006 (2018).

[74] J.-L. Wu, Y. Wang, J.-X. Han, S.-L. Su, Y. Xia, Y. Jiang, and J. Song, Unselective ground-state blockade of Rydberg atoms for implementing quantum gates, Front. Phys. **17**, 22501 (2022).

[75] It should be emphasized that, although Eqs. (3) and (5) exhibit different stark shifts, these undesired shifts must be eliminated through identical operations. This is because the control qubit's input states in quantum computation are often superposition states, and it would be an impractical approach to design separate operations to cancel the Stark shift in Eq. (3) versus Eq. (5). Our approach is outlined as follows: an additional pulse is applied to the target atom, resulting in the generation of $\Omega_b^2/\Delta(|r\rangle_t\langle r| - |b\rangle_t\langle b|)$. When the control qubit is $(|1\rangle)|0\rangle_c$ initially, it may not (or may) be excited to $|r\rangle_c$ and the generated Stark shift would be $\Omega_b^2/(4\Delta)(|(rr)0r\rangle\langle(rr)0r| - |(rb)0b\rangle\langle(rb)0b|)$. Therefore, both of the Stark shifts in the second line of Eqs. (3) and (5) are precisely canceled. For the third line in Eq. (3), one can add the microwave or electric field to induce the unresonant coupling between $|uv\rangle$ and $|rr\rangle$ to cancel it. This has no effect with the control qubit initially being in $|0\rangle$ since it would not be excited.

[76] X. Wang, M. Allegra, K. Jacobs, S. Lloyd, C. Lupo, and M. Mohseni, Quantum brachistochrone curves as geodesics: Obtaining accurate minimum-time protocols for the control of quantum systems, Phys. Rev. Lett. **114**, 170501 (2015).

[77] T. M. Graham, M. Kwon, B. Grinkemeyer, Z. Marra, X. Jiang, M. T. Lichtman, Y. Sun, M. Ebert, and M. Saffman, Rydberg-mediated entanglement in a two-dimensional neutral atom qubit array, Phys. Rev. Lett. **123**, 230501 (2019).

[78] H. Levine, A. Keesling, G. Semeghini, A. Omran, T. T. Wang, S. Ebadi, H. Bernien, M. Greiner, V. Vuletić, H. Pichler, and M. D. Lukin, Parallel implementation of high-fidelity multiqubit gates with neutral atoms, Phys. Rev. Lett. **123**, 170503 (2019).

[79] M. A. Nielsen, A simple formula for the average gate fidelity of a quantum dynamical operation, Phys. Lett. A **303**, 249 (2002).

[80] A. G. White, A. Gilchrist, G. J. Pryde, J. L. O'Brien, M. J. Bremner, and N. K. Langford, Measuring two-qubit gates, J. Opt. Soc. Am. B **24**, 172 (2007).

[81] X. Jiang, J. Scott, M. Friesen, and M. Saffman, Sensitivity of quantum gate fidelity to laser phase and intensity noise, Phys. Rev. A **107**, 042611 (2023).

[82] F. Riehle, *Frequency Standards: Basics and Applications* (John Wiley & Sons, New York, 2006).

[83] W. Lee, M. Kim, H. Jo, Y. Song, and J. Ahn, Coherent and dissipative dynamics of entangled few-body systems of Rydberg atoms, Phys. Rev. A **99**, 043404 (2019).

[84] I. S. Madjarov, J. P. Covey, A. L. Shaw, J. Choi, A. Kale, A. Cooper, H. Pichler, V. Schkolnik, J. R. Williams, and M. Endres, High-fidelity entanglement and detection of alkaline-earth Rydberg atoms, Nat. Phys. **16**, 857 (2020).

[85] X.-F. Shi, Suppressing motional dephasing of ground-Rydberg transition for high-fidelity quantum control with neutral atoms, Phys. Rev. Appl. **13**, 024008 (2020).

[86] L.-L. Yan, J.-W. Zhang, M.-R. Yun, J.-C. Li, G.-Y. Ding, J.-F. Wei, J.-T. Bu, B. Wang, L. Chen, S.-L. Su, F. Zhou, Y. Jia, E.-J. Liang, and M. Feng, Experimental verification of dissipation-time uncertainty relation, Phys. Rev. Lett. **128**, 050603 (2022).

[87] J. Samuel and R. Bhandari, General setting for berry's phase, Phys. Rev. Lett. **60**, 2339 (1988).

[88] J. Anandan and Y. Aharonov, Geometry of quantum evolution, Phys. Rev. Lett. **65**, 1697 (1990).

[89] D. N. Page, Geometrical description of berry's phase, Phys. Rev. A **36**, 3479 (1987).

[90] R. Scholtens, Optimized quantum state transitions : A survey of the quantum brachistochrone problem (unpublished).

[91] Y.-H. Kang, Y.-H. Chen, Z.-C. Shi, B.-H. Huang, J. Song, and Y. Xia, Nonadiabatic holonomic quantum computation using Rydberg blockade, Phys. Rev. A **97**, 042336 (2018).

[92] B.-J. Liu and M.-H. Yung, Leakage suppression for holonomic quantum gates, Phys. Rev. Appl. **14**, 034003 (2020).

[93] Y. Li, T. Xin, C. Qiu, K. Li, G. Liu, J. Li, Y. Wan, and D. Lu, Dynamical-invariant-based holonomic quantum gates: Theory and experiment, Fundamental Res. **3**, 229 (2023).

[94] T. Yan, B.-J. Liu, K. Xu, C. Song, S. Liu, Z. Zhang, H. Deng, Z. Yan, H. Rong, K. Huang, M.-H. Yung, Y. Chen, and D. Yu, Experimental realization of nonadiabatic shortcut to non-abelian geometric gates, Phys. Rev. Lett. **122**, 080501 (2019).

[95] A Ruschhaupt, X. Chen, D. Alonso, and J. G. Muga, Optimally robust shortcuts to population inversion in two-level quantum systems, New J. Phys. **14**, 093040 (2012).

[96] M. Li, F.-Q. Guo, Z. Jin, L.-L. Yan, E.-J. Liang, and S.-L. Su, Multiple-qubit controlled unitary quantum gate for Rydberg atoms using shortcut to adiabaticity and optimized geometric quantum operations, Phys. Rev. A **103**, 062607 (2021).

[97] J. Niu, B.-J. Liu, Y. Zhou, T. Yan, W. Huang, W. Liu, L. Zhang, H. Jia, S. Liu, M.-H. Yung, Y. Chen, and D. Yu, Customizable quantum control via stimulated raman user-defined passage, Phys. Rev. Appl. **17**, 034056 (2022).